Mitigation of Oscillations in Three Phase *LCL*-Filtered Grid Converters Based on Proportional Resonance and Improved Model Predictive Control

Qi Geng, Huadong Sun, Xing Zhang, Xiaoxin Zhou, *Fellow, IEEE,* Jun Liang, *Senior Member, IEEE,* Yi Geng

***Abstract*—For three phase *LCL*-filtered gird converters, this paper designs a robust control strategy to reduce high frequency and subsynchronous or supersynchronous oscillations. Two components, namely the grid side inductor component and the *LC* filter component, constitute a three phase *LCL*-filtered grid converter. Model predictive control (MPC) with a disturbance observer is used to control the interconnection voltage of the *LC* filter. Proportional resonance (PR) control regulates the grid side current. It is possible to combine MPC with PR's advantages. The dynamic performance is enhanced by MPC's intrinsic ability to achieve active damping without extra control and reduce modulation latency. In addition to achieving zero steady state error, PR control greatly simplifies the control process when compared to the overall MPC of the entire grid converter. By analyzing the frequency response of the transfer function and output impedance, it is possible to determine that the proposed control has a sufficient phase margin and that, even when the system and control parameters change, the grid converters' output impedance is always resistive or inductive at the entire frequency, suppressing subsynchronous and high frequency oscillations. To further reduce the oscillations and harmonics, an improved MPC control framework and a feedback compensation mechanism are proposed. The effectiveness and reliability of the proposed control in current tracking, harmonic suppression, and response to grid impedance variations are verified by comparative analysis of simulation results.**

***Index Terms*—model predictive control, voltage source converter, *LCL*, oscillation**

I. Introduction

The control performance of grid connected converters has emerged as the primary determinant of power quality [1]-[4] as more renewable energy is penetrated into the power grid. Due to its frequent switching, grid converters as power electronic devices introduce a significant amount of harmonics into the grid, which causes grid operation instability [5]. According to the DC side component, grid connected converters are divided into voltage source converters (VSC) and current source converters (CSC). Since CSC's huge inductance will negatively affect dynamic performance, VSC is frequently employed in real-world control. The grid converters are connected to the grid through filters in order to reduce the harmonics of the grid side current. The typical filter is an *L* filter, which effectively suppresses high-order harmonics due to its high frequency attenuation capability [6]. However, the *L* filter's high inductance increases both the size and expense of the equipment. Due to its small size and capacity for attenuating high frequency harmonics, *LCL* filters are frequently utilized. Because of the low capacitive reactance at high frequencies, high-order harmonics can be filtered out. Additionally, because of the huge capacitive reactance at low frequencies, the power frequency response is unaffected. However, the *LCL* filter will produce high frequency resonance; the amplitude-frequency response of the filter exhibits a resonance peak at the resonance frequency, and the phase-frequency response exhibits a phase jump at the resonance frequency [7].

For an *LCL* filter, there are two different damping techniques. One is passive damping by altering the circuit structure, which brings the additional power losses [8]-[10]. The other is active damping, which can be divided into single-loop [11]-[13] and multi-loop active damping [14]-[16]. The current control method with filters is used in single-loop active damping to squelch high frequency resonance. However, changes in gird impedance will alter the resonance frequency and reduce the effectiveness of single-loop active damping. The limitations of the traditional single-loop control can be overcome by the multiloop control since it naturally dampens the VSC system. The state feedback control known as multi-loop active damping adds proportional or proportional-derivative state feedback to the modulation signal to create a virtual impedance. However, the choose of feedback state and the tunning of multi-loop control are complicated.

Active damping and grid converter current control are two applications of the emerging MPC [17]. [18] studied active damping using finite control set model predictive control (FSC-MPC) with multi state feedback. However, active damping's design is intricate. Active damping will be required if the converter side current serves as the control variable. Long prediction horizons of MPC without active damping are utilized when the grid side current is the control variable, which increases the computing cost [19]-[20]. In order to regulate the overall grid converter with *LCL* filter, [21] investigated a nearly optimal FSC-MPC, but the weighting factor tuning is intricate.

If the control settings are not properly chosen, it may also result in supersynchronous or subsynchronous oscillations in addition to high frequency oscillation. The frequency response of grid inverter output impedance close to the power frequency is most affected by PLL proportional and integral gains,

This work was supported by the National Natural Science Foundation of China under Grant U2066602.

Qi Geng, Huadong Sun, Xing Zhang, and Xiaoxin Zhou are with China Electric Power Research Institute (CEPRI), Beijing, 100192, China (email: 707065428@qq.com).

Jun Liang is with the School of Engineering, Cardiff University, Cardiff CF24 3AA, U.K..

Yi Geng is with the School of Microelectronics, Tianjin University, Tianjin, 300072, China.

whereas the frequency response of subsynchronous and supersynchronous frequency is influenced by the proportional and integral gains of the current controller. To date, there hasn't been any relevant research on model predictive control's effectiveness in reducing the subsynchronous oscillations of *LCL*-filtered grid converters.

This paper proposes a robust control strategy for three phase *LCL*-filtered gird converters to reduce high frequency and subsynchronous or supersynchronous oscillations, which is motivated by the aforementioned restrictions. Two components, an *LC* filter and a grid side inductor, make up a three phase *LCL*-filtered grid converter. Model predictive control (MPC) with a disturbance observer is used to control the interconnection voltage of the *LC* filter. The grid side current is regulated by proportional resonance (PR) control. The advantages of MPC and PR can therefore be combined. The dynamic performance is enhanced by MPC's intrinsic ability to achieve active damping without extra control and reduce modulation latency. PR control not only makes the steady state error zero, but also reduces the complexity of control compared with the overall MPC of the entire grid converter.

Additionally, the conventional MPC's variable switching frequency and prediction inaccuracy will result in more oscillations and harmonics. The *LCL*-filtered converter is controlled by the proposed method with conventional MPC in [1], and the findings demonstrate that, in terms of steady and dynamic performance, the proposed control outperforms PR control with active damping and PI control without active damping. On the basis of the methodology in [1], we propose complementary strategies in this paper: 1) An improved MPC control framework is designed to decrease the harmonics. 2) A feedback compensation method for MPC is proposed to enhance delay synchronization and output prediction, hence reducing the tracking error and the resulting oscillations and harmonics. 3) Compared with conventional MPC, the proposed improved MPC can largely reduce switching frequency and total harmonic distortion (THD) of the output voltage by selecting the optimal control parameters.

The rest of this paper is organized as follows. In Section II, the conventional and improved MPC of *LC* filter component is described in detail. Section III gives an MPC scheme with disturbance observer. Section IV presents the frequency response of the proposed proportional resonance and model predictive control, where its superior dynamic performance and robustness are analyzed. This is followed by the analysis of the simulation results in Section V, and the effectiveness and rationality of the proposed control is confirmed. Finally, we draw the conclusions in Section VI.

II. MPC OF *LC* FILTER COMPONENT

In Fig. 1, three phase *LCL*-filtered grid converter is divided into two components, *LC* filter and grid side inductor. The interconnection voltage u_i of *LC* filter is regulated by MPC. The grid side current is regulated by PR control.

A. Predictive Model of Interconnection Voltage

The state-space model of *LC* filter in the *dq* reference frame is first built.

$$d\boldsymbol{x}/dt = A\boldsymbol{x} + B\boldsymbol{u} \tag{1}$$

$$\boldsymbol{y} = C\boldsymbol{x} \tag{2}$$

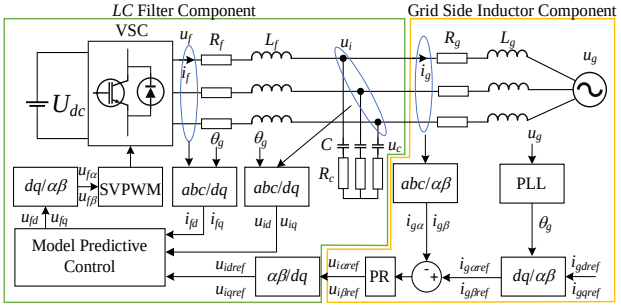

Fig. 1. Proportional resonance and model predictive control of three phase LCL-filtered grid converter.

$$\frac{di_{gd}}{dt} = a_d u_{id} + b_d u_{gd} + c_d i_{gd} + d_d i_{gq} \tag{3}$$

$$\frac{di_{gq}}{dt} = a_q u_{iq} + b_q u_{gq} + c_q i_{gq} + d_q i_{gd} \tag{4}$$

with

$$A = \begin{bmatrix} -\frac{R_f+R_c}{L_f} & \omega_s & -\frac{1}{L_f} & 0 & \frac{R_c}{L_f} & 0 & 0 & 0 \\ -\omega_s & -\frac{R_f+R_c}{L_f} & 0 & -\frac{1}{L_f} & 0 & \frac{R_c}{L_f} & 0 & 0 \\ \frac{1}{C} & 0 & 0 & \omega_s & -\frac{1}{C} & 0 & 0 & 0 \\ 0 & \frac{1}{C} & -\omega_s & 0 & 0 & -\frac{1}{C} & 0 & 0 \\ 0 & 0 & 0 & 0 & 0 & 0 & 1 & 0 \\ 0 & 0 & 0 & 0 & 0 & 0 & 0 & 1 \\ 0 & 0 & 0 & 0 & 0 & 0 & 0 & 0 \\ 0 & 0 & 0 & 0 & 0 & 0 & 0 & 0 \end{bmatrix} \quad B = \begin{bmatrix} \frac{1}{L_f} & 0 \\ 0 & \frac{1}{L_f} \\ 0 & 0 \\ 0 & 0 \\ 0 & 0 \\ 0 & 0 \\ 0 & 0 \\ 0 & 0 \end{bmatrix}$$

$$C = \begin{bmatrix} R_c & 0 & 1 & 0 & -R_c & 0 & 0 & 0 \\ 0 & R_c & 0 & 1 & 0 & -R_c & 0 & 0 \end{bmatrix}$$

$a_d = a_q = 1/L_g \quad b_d = b_q = -1/L_g \quad c_d = c_q = -R_g/L_g \quad d_d = d_q = \omega_s$

where L_f and R_f are the converter side inductance and resistance, L_g and R_g are the grid side inductance and resistance, C and $\boldsymbol{R}_c$ are the filter capacitance and charging resistance. $\boldsymbol{x} = \begin{bmatrix} i_{fd} & i_{fq} & u_{cd} & u_{cq} & i_{gd} & i_{gq} & d_{gd} & d_{gq} \end{bmatrix}^T$, $\boldsymbol{u} = \begin{bmatrix} u_{fd} & u_{fq} \end{bmatrix}^T$, $\boldsymbol{y} = \begin{bmatrix} u_{id} & u_{iq} \end{bmatrix}^T$ represent the state, input, and output vector. i_{fd} and i_{fq} are the converter side current, i_{gd} and i_{gq} are the grid side current, d_{gd} and d_{gq} are the derivative of the grid side current, $d_{gd} = di_{gd}/dt$, $d_{gq} = di_{gq}/dt$. u_{cd} and u_{cq} are the capacitor voltage, u_{id} and u_{iq} are the interconnection voltage, u_{fd} and u_{fq} are the output voltage of the converter. ω_s is the gird rated angular frequency.

The state space model (1)-(4) shall be represented in the discrete time domain through zero order hold circuit to apply MPC. The discrete state space model is

$$\boldsymbol{x}(k+1) = A_D \boldsymbol{x}(k) + B_D \boldsymbol{u}(k) \tag{5}$$

$$\boldsymbol{y}(k) = C_D \boldsymbol{x}(k) \tag{6}$$

$$i_{gd}(k+1)=a_{dD}u_{id}(k)+b_{dD}u_{gd}(k)+c_{dD}i_{gd}(k)+d_{dD}i_{gq}(k) \tag{7}$$

$$i_{gq}(k+1)=a_{qD}u_{id}(k)+b_{qD}u_{gd}(k)+c_{qD}i_{gd}(k)+d_{qD}i_{gq}(k) \tag{8}$$

with

$$A_D=e^{AT}\approx\begin{bmatrix} 1-\frac{T(R_f+R_c)}{L_f} & \omega_s T & -\frac{T}{L_f} & 0 & \frac{R_c T}{L_f} & 0 & 0 & 0 \\ -\omega_s T & 1-\frac{T(R_f+R_c)}{L_f} & 0 & -\frac{T}{L_f} & 0 & \frac{R_c T}{L_f} & 0 & 0 \\ \frac{T}{C} & 0 & 1 & \omega_s T & -\frac{T}{C} & 0 & 0 & 0 \\ 0 & \frac{T}{C} & -\omega_s T & 1 & 0 & -\frac{T}{C} & 0 & 0 \\ 0 & 0 & 0 & 0 & 1 & 0 & T & 0 \\ 0 & 0 & 0 & 0 & 0 & 1 & 0 & T \\ 0 & 0 & 0 & 0 & 0 & 0 & 1 & 0 \\ 0 & 0 & 0 & 0 & 0 & 0 & 0 & 1 \end{bmatrix}$$

$$B_D=\int_0^T e^{A\tau}d\tau\cdot B\approx\begin{bmatrix} \frac{T}{L_f} & 0 \\ 0 & \frac{T}{L_f} \\ 0 & 0 \\ 0 & 0 \\ 0 & 0 \\ 0 & 0 \\ 0 & 0 \\ 0 & 0 \end{bmatrix}$$

$$C_D=C$$

$$a_{dD}=a_{qD}=\frac{T}{L_g}$$

$$b_{dD}=b_{qD}=-\frac{T}{L_g}$$

$$c_{dD}=c_{qD}=1-\frac{TR_g}{L_g}$$

$$d_{dD}=d_{qD}=\omega_s T$$

where A_D, B_D, C_D, a_{dD}, a_{qD}, b_{dD}, b_{qD}, c_{dD}, c_{qD}, d_{dD}, d_{qD} are the discrete matrices and coefficients with a sampling period *T*.

The interconnection voltage in (6) is represented by

$$\begin{aligned} u_{id}(k+1)&=C_{D1}\boldsymbol{x}(k+1)=R_c i_{fd}(k+1)+u_{cd}(k+1)-R_c i_{gd}(k+1)= \\ &\alpha u_{cd}(k)+\beta u_{cq}(k)+\gamma u_{fd}(k)+\delta i_{fd}(k)+\varphi i_{fq}(k)+\zeta i_{gd}(k)+\lambda d_{gd}(k) \end{aligned} \tag{9}$$

$$\begin{aligned} u_{iq}(k+1)&=C_{D2}\boldsymbol{x}(k+1)=R_c i_{fq}(k+1)+u_{cq}(k+1)-R_c i_{gq}(k+1)= \\ &\alpha u_{cq}(k)-\beta u_{cd}(k)+\gamma u_{fq}(k)+\delta i_{fq}(k)-\varphi i_{fd}(k)+\zeta i_{gq}(k)+\lambda d_{gq}(k) \end{aligned} \tag{10}$$

with

$$\alpha=1-\frac{R_c T}{L_f}\quad \beta=\omega_s T\quad \gamma=\frac{R_c T}{L_f}\quad \delta=R_c\left[1-\frac{T(R_c+R_f)}{L_f}\right]+\frac{T}{C}$$

$$\varphi=R_c\omega_s T\quad \zeta=R_c\left(\frac{R_c T}{L_f}-1\right)-\frac{T}{C}\quad \lambda=-R_c T$$

where C_{D1} and C_{D2} are the first and the second row of C_D.

Substitute (6) into (9) and (10), we can get

$$\begin{aligned} u_{id}(k+1)&=\alpha u_{id}(k)+\beta u_{iq}(k)+\gamma u_{fd}(k)+ \\ &\tilde{\delta} i_{fd}(k)+\tilde{\zeta} i_{gd}(k)+\phi i_{gq}(k)+\lambda d_{gd}(k) \end{aligned} \tag{11}$$

$$\begin{aligned} u_{iq}(k+1)&=\alpha u_{iq}(k)-\beta u_{id}(k)+\gamma u_{fq}(k)+ \\ &\tilde{\delta} i_{fq}(k)+\tilde{\zeta} i_{gq}(k)-\phi i_{gd}(k)+\lambda d_{gq}(k) \end{aligned} \tag{12}$$

with $\tilde{\delta}=-\frac{R_c R_f T}{L_f}+\frac{T}{C}$, $\tilde{\zeta}=-\frac{T}{C}$, $\phi=-R_c\omega_s T$.

The discrete interconnection voltage predictive model is

$$\begin{aligned} u_{id}(k+1)&=u_{id}(k)+(\alpha-1)u_{id}(k)+\beta u_{iq}(k)+ \\ &\gamma u_{fd}(k)+\tilde{\delta} i_{fd}(k)+\tilde{\zeta} i_{gd}(k)+\phi i_{gq}(k)+\lambda d_{gd}(k) \end{aligned} \tag{13}$$

$$\begin{aligned} u_{iq}(k+1)&=u_{iq}(k)+(\alpha-1)u_{iq}(k)-\beta u_{id}(k)+ \\ &\gamma u_{fq}(k)+\tilde{\delta} i_{fq}(k)+\tilde{\zeta} i_{gq}(k)-\phi i_{gd}(k)+\lambda d_{gq}(k) \end{aligned} \tag{14}$$

The converter voltage u_{fd} and u_{fq} is defined as

$$u_{fd}(k)=u_{fd}(k-1)+\Delta u_{fd}(k) \tag{15}$$

$$u_{fq}(k)=u_{fq}(k-1)+\Delta u_{fq}(k) \tag{16}$$

where $\Delta u_{fd}(k)$ and $\Delta u_{fq}(k)$ are the variations of the *dq* component of converter voltage from $(k-1)^{\text{th}}$ to k^{th} period.

Substitute (15) and (16) into (13) and (14), we get

$$\begin{aligned} u_{id}(k+1)&=u_{id}(k)+(\alpha-1)u_{id}(k)+\beta u_{iq}(k)+\gamma u_{fd}(k-1)+ \\ &\gamma\Delta u_{fd}(k)+\tilde{\delta} i_{fd}(k)+\tilde{\zeta} i_{gd}(k)+\phi i_{gq}(k)+\lambda d_{gd}(k) \end{aligned} \tag{17}$$

$$\begin{aligned} u_{iq}(k+1)&=u_{iq}(k)+(\alpha-1)u_{iq}(k)-\beta u_{id}(k)+\gamma u_{fq}(k-1)+ \\ &\gamma\Delta u_{fq}(k)+\tilde{\delta} i_{fq}(k)+\tilde{\zeta} i_{gq}(k)-\phi i_{gd}(k)+\lambda d_{gq}(k) \end{aligned} \tag{18}$$

Define the cost function in k^{th} prediction horizon as

$$\begin{aligned} \min J(k)=&\left[u_{idref}(k+1)-u_{id}(k+1)\right]^2+\left[u_{iqref}(k+1)-u_{iq}(k+1)\right]^2+ \\ &\Delta u_{fd}(k)^2+\Delta u_{fq}(k)^2 \end{aligned} \tag{19}$$

where u_{idref} and u_{iqref} are the reference of the interconnection voltage. The first two terms of $J(k)$ guarantees the predictive output vector $\boldsymbol{y}(k+1)$ can track the references to minimize the tracking error. The remaining terms of $J(k)$ minimizes the variation of the input vector $\boldsymbol{u}(k)$.

Differentiating the cost function $J(k)$ with respect to $\Delta u_{fd}(k)$ and $\Delta u_{fq}(k)$, we have

$$\begin{aligned} \frac{\partial J(k)}{\partial\Delta u_{fd}(k)}&=2\left[-\gamma u_{idref}(k+1)+\gamma u_{id}(k+1)+\Delta u_{fd}(k)\right]=0 \\ \frac{\partial J(k)}{\partial\Delta u_{fq}(k)}&=2\left[-\gamma u_{iqref}(k+1)+\gamma u_{iq}(k+1)+\Delta u_{fq}(k)\right]=0 \end{aligned} \tag{20}$$

The variations of the *dq* component of converter voltage are

$$\begin{aligned} \Delta u_{fd}(k)&=\gamma\left[u_{idref}(k+1)-u_{id}(k+1)\right] \\ \Delta u_{fq}(k)&=\gamma\left[u_{iqref}(k+1)-u_{iq}(k+1)\right] \end{aligned} \tag{21}$$

Substitute (21) into (17) and (18), the predictive model of the interconnection voltage is

$$u_{id}(k+1)=\begin{bmatrix} u_{id}(k)+(\alpha-1)u_{id}(k)+\beta u_{iq}(k)+\gamma u_{fd}(k-1)+ \\ \gamma^2 u_{idref}(k+1)+\tilde{\delta} i_{fd}(k)+\tilde{\zeta} i_{gd}(k)+\phi i_{gq}(k)+\lambda d_{gd}(k) \end{bmatrix}\Big/\left(1+\gamma^2\right) \tag{22}$$

$$u_{iq}(k+1)=\begin{bmatrix} u_{iq}(k)+(\alpha-1)u_{iq}(k)-\beta u_{id}(k)+\gamma u_{fq}(k-1)+ \\ \gamma^2 u_{iqref}(k+1)+\tilde{\delta} i_{fq}(k)+\tilde{\zeta} i_{gq}(k)-\phi i_{gd}(k)+\lambda d_{gq}(k) \end{bmatrix}\Big/\left(1+\gamma^2\right) \tag{23}$$

B. Improved Model Predictive Control

For the purpose of further decreasing the computational loads and facilitating the analysis, we propose a single-step forecast method in the MPC scheme in this section. At the start of each control interval, the variables of state are sampled and the switch of the system is realized by the controller at the same time. In the practical implementation, taking into account the unneglectable characteristic of the computation time and acquisition time, the traditional MPC method is executed in the subsequent step to balance out the latency time. First of all, the

converter side current i_f, the capacitor voltage u_c, and the grid side current i_g at kT are quantified, followed by the forecast of state variables at $(k+1)T$ considering the switch action delay of controllers based on the output voltage of the converter and the discrete state space model (5). Next, the output voltage of *LC* filter for all possible voltage vectors in the finite control set at the $(k+2)T$ sampling point is forecasted. Lastly, the forecasted values of all voltage vectors are assessed by utilizing the defined cost function. Then the associated state of switch will be chosen from all possible voltage vectors to minimize the value of the cost function.

It is worth mentioning that the cost function should include the control effort and the deviations of the desired output state and the actual output state under MPC-based control. Furthermore, in the improved MPC, the weights of various control objectives should be incorporated in the new cost function, consequently it is intuitively plausible for us to adjust and optimize the control objectives [22]. In the improved MPC, the proposed cost function is expressed as follow:

$$J = J_o + \lambda_{dif} J_{dif} + \lambda_{sw} J_{sw} + i_{con} \tag{24}$$

where the first term J_o ensures the predictive output voltage can track the references to minimize the tracking error, J_{dif} represents the term of the differential to the capacitor voltage, J_{sw} is the punishment of switch control effort. λ_{dif} and λ_{sw} are the weighted factor respectively for J_{dif} and J_{sw}. It is important to note that the weighted factors are simplified to λ_{dif} and λ_{sw} can promote analysis and tuning while greatly improving the calculation speed in the processor. i_{con} is the limitation of the converter side current, if $i_f > i_{f\max}$, $i_{con} = \infty$; else, $i_{con} = 0$. $i_{f\max}$ is the current upper bound.

In (24), the tracking error term of the forecasted output voltage can be expresses by:

$$J_o = \left(u_{cref} - u_c\right)^2 \tag{25}$$

where u_{cref} is the reference of the capacitor voltage, u_c is the forecasted output capacitor voltage at $(k+2)T$.

It can be seen from the dynamics of *LCL*-filtered converters that tracking voltage and the derivative of voltage can enable the system to be controlled efficiently, which is better-off than the control only tracking voltage. The reference of capacitor voltage can be represented by:

$$\begin{aligned} u_{c\alpha}^* &= u_{cref} \sin\left(\omega_{ref} t\right) \\ u_{c\beta}^* &= u_{cref} \cos\left(\omega_{ref} t\right) \end{aligned} \tag{26}$$

The derivative of the capacitor voltage reference is

$$\begin{aligned} \frac{du_{c\alpha}^*}{dt} &= \omega_{ref} u_{cref} \cos\left(\omega_{ref} t\right) = \omega_{ref} u_{c\beta}^* \\ \frac{du_{c\beta}^*}{dt} &= -\omega_{ref} u_{cref} \sin\left(\omega_{ref} t\right) = -\omega_{ref} u_{c\alpha}^* \end{aligned} \tag{27}$$

The derivative of the capacitor voltage according to the dynamics of capacitor can be described as:

$$\begin{aligned} \frac{du_{c\alpha}}{dt} &= \frac{i_{f\alpha} - i_{g\alpha}}{C_f} \\ \frac{du_{c\beta}}{dt} &= -\frac{i_{f\beta} - i_{g\beta}}{C_f} \end{aligned} \tag{28}$$

By subtracting (28) from (27), the tracking deviation of the derivative of the capacitor voltage can be derived. With a focus on convenience for operating on computer, we multiply the capacitor C_f at each side.

$$J_{dif} = \left(\omega_{ref} C_f u_{c\beta}^* - i_{f\alpha} + i_{g\alpha}\right)^2 + \left(\omega_{ref} C_f u_{c\alpha}^* + i_{f\beta} - i_{g\beta}\right)^2 \tag{29}$$

The punishment term of switch control J_{sw} can decrease the switching frequency, which can be written as:

$$J_{sw} = \frac{\sum_{i=a,b,c} \left|S_i(k+1) - S_i(k)\right|}{3 \times 2} \tag{30}$$

where S_i represents the switch disposition of the corresponding phase.

C. Feedback Compensation

In order to further reduce the tracking error, we can adopt methods to decrease the forecast deviation in addition to adding extra limitations in the cost function.

As shown in Fig. 2, considering delay synchronization, the forecast values with slight variation may prefer different selection for the optimal switching patterns, for example $u_{for1}(k+1)$ and $u_{for2}(k+1)$. Consequently, reducing the forecast error of delay synchronization is an effective way to improve the tracking performance, which can be helpful for suppressing the resulting oscillations and harmonics.

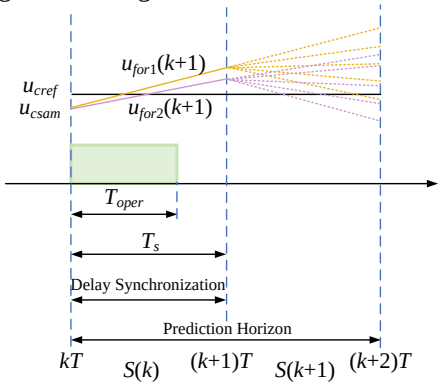

Fig. 2. Analysis of feedback compensation.

In comparison to the control cycle, the basic cyclic error alters at a glacial pace, which can be estimated as:

$$u_{err}(k+1) = u_{for}(k) - u_{sam}(k) \tag{31}$$

where $u_{sam}(k)$ is sampled data of the capacitor voltage at kT, $u_{for}(k)$ is the forecast capacitor voltage at kT from the previous control period. Therefore, the compensation value of the forecast voltage utilized for delay synchronization can be derived as

$$u_{com}(k+1) = u_{for}(k+1) - \lambda_c u_{err}(k+1) \tag{32}$$

where $u_{for}(k+1)$ is the forecast voltage obtained by the discrete state space model, λ_c is the factor of feedback compensation.

III. MPC WITH STATE OBSERVER

A. Impact of L_f, R_f, and C Variation on the Prediction Model

L_f, R_f, and C may vary in the practical *LCL* filtered grid converters. The discrete interconnection voltage predictive model in *dq* frame considering parameters variation is

$$\bar{u}_{id}(k+1)=u_{id}(k)+\frac{T}{L_f+\Delta L_f}\left[-R_c u_{id}(k)+\omega_s\left(L_f+\Delta L_f\right)u_{iq}(k)+R_c u_{fd}(k)\right]+ \quad (33)$$
$$T\left(\frac{1}{C+\Delta C}-\frac{R_c\left(R_f+\Delta R_f\right)}{L_f+\Delta L_f}\right)i_{fd}(k)-\frac{T}{C+\Delta C}i_{gd}(k)+\phi i_{gq}(k)+\lambda d_{gd}(k)$$

$$\bar{u}_{iq}(k+1)=u_{iq}(k)+\frac{T}{L_f+\Delta L_f}\left[-R_c u_{iq}(k)-\omega_s\left(L_f+\Delta L_f\right)u_{id}(k)+R_c u_{fq}(k)\right]+ \quad (34)$$
$$T\left(\frac{1}{C+\Delta C}-\frac{R_c\left(R_f+\Delta R_f\right)}{L_f+\Delta L_f}\right)i_{fq}(k)-\frac{T}{C+\Delta C}i_{gq}(k)-\phi i_{gd}(k)+\lambda d_{gq}(k)$$

(13) and (14) respectively subtract (33) and (34), the impact of the parameters variation on the prediction model are

$$e_{id}(k+1)=\varepsilon_1 u_{id}(k)+\varepsilon_2 u_{fd}(k)+\varepsilon_3 i_{fd}(k)+\varepsilon_4 i_{gd}(k) \quad (35)$$

$$e_{iq}(k+1)=\varepsilon_1 u_{iq}(k)+\varepsilon_2 u_{fq}(k)+\varepsilon_3 i_{fq}(k)+\varepsilon_4 i_{gq}(k) \quad (36)$$

with

$$\varepsilon_1=\frac{-R_c T\Delta L_f}{L_f\left(L_f+\Delta L_f\right)}\quad \varepsilon_2=\frac{R_c T\Delta L_f}{L_f\left(L_f+\Delta L_f\right)}\quad \varepsilon_3=\frac{T\Delta C}{C(C+\Delta C)}+\frac{T\left(R_c L_f\Delta R_f-R_c R_f\Delta L_f\right)}{L_f\left(L_f+\Delta L_f\right)}\quad \varepsilon_4=-\frac{T\Delta C}{C(C+\Delta C)}$$

where e_{id} and e_{iq} are the prediction error of the interconnection voltage, ΔL_f, ΔR_f, and ΔC are the variations of the converter side inductance, resistance and capacitance.

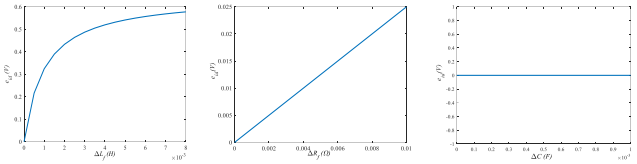

(a) (b) (c)

Fig. 3. Impact of (a) L_f, (b) R_f, and (c) C error on the prediction interconnection voltage.

As depicted in Fig. 3, the prediction error grows with the increase of L_f and R_f, and ΔL_f has a greater influence than ΔR_f. Since $i_{fd}\approx i_{gd}$, the impact of ΔC in ε_3 and ε_4 cancel each other out and the prediction error is not affected by the filter capacitance. The parameter variations worsen the control performance when they are over certain values. For example, the frequency of resonance will change. Hence, it is necessary to add disturbance rejection control link in MPC to enhance the robustness to parameter variations.

B. Disturbance Observer

The interconnection voltage dynamics are

$$L_f\frac{du_{id}}{dt}=-R_c u_{id}+\omega_s\left(L_f+\Delta L_f\right)u_{iq}+R_c u_{fd}+\left(\frac{L_f+\Delta L_f}{C+\Delta C}-R_c\left(R_f+\Delta R_f\right)\right)i_{fd}- \quad (37)$$
$$\frac{L_f+\Delta L_f}{C+\Delta C}i_{gd}-R_c\omega_s\left(L_f+\Delta L_f\right)i_{gq}-R_c\left(L_f+\Delta L_f\right)d_{gd}-\Delta L_f\frac{du_{id}}{dt}$$

$$L_f\frac{du_{iq}}{dt}=-R_c u_{iq}-\omega_s\left(L_f+\Delta L_f\right)u_{id}+R_c u_{fq}+\left(\frac{L_f+\Delta L_f}{C+\Delta C}-R_c\left(R_f+\Delta R_f\right)\right)i_{fq}- \quad (38)$$
$$\frac{L_f+\Delta L_f}{C+\Delta C}i_{gq}+R_c\omega_s\left(L_f+\Delta L_f\right)i_{gd}-R_c\left(L_f+\Delta L_f\right)d_{gq}-\Delta L_f\frac{du_{iq}}{dt}$$

The converter voltage u_{fd} and u_{fq} are the input variables, and all other terms are considered as the lump of disturbances f_d and f_q imposed on u_{id} and u_{iq} dynamics.

$$f_d=\frac{1}{L_f}\left[\begin{array}{l}-R_c u_{id}+\omega_s\left(L_f+\Delta L_f\right)u_{iq}+\left(\frac{L_f+\Delta L_f}{C+\Delta C}-R_c\left(R_f+\Delta R_f\right)\right)i_{fd}-\\ \frac{L_f+\Delta L_f}{C+\Delta C}i_{gd}-R_c\omega_s\left(L_f+\Delta L_f\right)i_{gq}-R_c\left(L_f+\Delta L_f\right)d_{gd}-\Delta L_f\frac{du_{id}}{dt}\end{array}\right] \quad (39)$$

$$f_q=\frac{1}{L_f}\left[\begin{array}{l}-R_c u_{iq}-\omega_s\left(L_f+\Delta L_f\right)u_{id}+\left(\frac{L_f+\Delta L_f}{C+\Delta C}-R_c\left(R_f+\Delta R_f\right)\right)i_{fq}-\\ \frac{L_f+\Delta L_f}{C+\Delta C}i_{gq}+R_c\omega_s\left(L_f+\Delta L_f\right)i_{gd}-R_c\left(L_f+\Delta L_f\right)d_{gq}-\Delta L_f\frac{du_{iq}}{dt}\end{array}\right] \quad (40)$$

The state space model with the lump of disturbances is

$$\begin{aligned}\dot{\boldsymbol{x}}_{DO}&=A_{DO}\boldsymbol{x}_{DO}+B_{DO}\boldsymbol{u}_{DO}+E\boldsymbol{h}\\ \boldsymbol{y}_{DO}&=C_{DO}\boldsymbol{x}_{DO}\end{aligned} \quad (41)$$

with

$$A_{DO}=\begin{bmatrix}0&0&1&0\\0&0&0&1\\0&0&0&0\\0&0&0&0\end{bmatrix}\quad B_{DO}=\begin{bmatrix}R_c/L_f&0\\0&R_c/L_f\\0&0\\0&0\end{bmatrix}\quad E=\begin{bmatrix}0&0\\0&0\\1&0\\0&1\end{bmatrix}\quad C_{DO}=\begin{bmatrix}1&0\\0&1\\0&0\\0&0\end{bmatrix}^T$$

where the state vector $\boldsymbol{x}_{DO}=\begin{bmatrix}x_{1d}&x_{1q}&x_{2d}&x_{2q}\end{bmatrix}^T$, $x_{1d}=u_{id}$, $x_{1q}=u_{iq}$, $x_{2d}=f_d$, $x_{2q}=f_q$, the input vector $\boldsymbol{u}_{DO}=\begin{bmatrix}u_{fd}&u_{fq}\end{bmatrix}^T$, $h_{DO}=\begin{bmatrix}h_d&h_q\end{bmatrix}^T$, $h_d=\dot{f}_d$, $h_q=\dot{f}_q$, the output vector $\boldsymbol{y}_{DO}=\begin{bmatrix}x_{1d}&x_{1q}\end{bmatrix}^T$.

Construct Luenberger observer as

$$\begin{aligned}\dot{\hat{\boldsymbol{x}}}_{DO}&=A_{DO}\hat{\boldsymbol{x}}_{DO}+B_{DO}\boldsymbol{u}_{DO}+L\left(\boldsymbol{y}-\hat{\boldsymbol{y}}\right)\\ \hat{\boldsymbol{y}}_{DO}&=C_{DO}\hat{\boldsymbol{x}}_{DO}\end{aligned} \quad (42)$$

with

$$L=\begin{bmatrix}-\beta_{1d}&0&-\beta_{2d}&0\\0&-\beta_{1q}&0&-\beta_{2q}\end{bmatrix}^T$$

where $\hat{\boldsymbol{x}}_{DO}=\begin{bmatrix}\hat{x}_{1d}&\hat{x}_{1q}&\hat{x}_{2d}&\hat{x}_{2q}\end{bmatrix}^T$ is the estimated state vector, $\hat{\boldsymbol{y}}_{DO}=\begin{bmatrix}\hat{x}_{1d}&\hat{x}_{1q}\end{bmatrix}^T$ is the estimated output vector.

The discrete state space model of (42) is

$$\hat{\boldsymbol{x}}_{DO}(k+1)=A_{DOD}\hat{\boldsymbol{x}}_{DO}(k)+B_{DOD}\boldsymbol{u}_{DO}(k)+\left(LC_{DO}\right)_D\left(\boldsymbol{x}_{DO}(k)-\hat{\boldsymbol{x}}_{DO}(k)\right) \quad (43)$$

with

$$A_{DOD}=\begin{bmatrix}1&0&T&0\\0&1&0&T\\0&0&1&0\\0&0&0&1\end{bmatrix}\quad B_{DOD}=\begin{bmatrix}TR_c/L_f&0\\0&TR_c/L_f\\0&0\\0&0\end{bmatrix}$$

$$\left(LC_{DO}\right)_D=\begin{bmatrix}-T\beta_{1d}&0&0&0\\0&-T\beta_{1q}&0&0\\-T\beta_{2d}&0&0&0\\0&-T\beta_{2q}&0&0\end{bmatrix}$$

The component wise of (43) are

$$\begin{aligned}\hat{x}_{1d}(k+1)&=\hat{x}_{1d}(k)+T\hat{x}_{2d}(k)+\frac{TR_c}{L_f}u_{fd}(k)-T\beta_{1d}\left(\hat{x}_{1d}(k)-x_{1d}(k)\right)\\ \hat{x}_{1q}(k+1)&=\hat{x}_{1q}(k)+T\hat{x}_{2q}(k)+\frac{TR_c}{L_f}u_{fq}(k)-T\beta_{1q}\left(\hat{x}_{1q}(k)-x_{1q}(k)\right)\\ \hat{x}_{2d}(k+1)&=\hat{x}_{2d}(k)-T\beta_{2d}\left(\hat{x}_{1d}(k)-x_{1d}(k)\right)\\ \hat{x}_{2q}(k+1)&=\hat{x}_{2q}(k)-T\beta_{2q}\left(\hat{x}_{1q}(k)-x_{1q}(k)\right)\end{aligned} \quad (44)$$

The aim of the disturbance observer is to estimate the lump of disturbances and introduce compensation of the parameters variation into control to realize the complete control of the disturbance. Substitute the estimated lump of disturbances $\hat{x}_{2d}$ and $\hat{x}_{2q}$ into (37) and (38), the converter voltage is

$$\begin{aligned} u_{fd}(k) &= \frac{L_f}{R_c T}\left[u_{idref}(k+1) - u_{id}(k+1)\right] - \frac{L_f}{R_c}\hat{x}_{2d}(k) \\ u_{fq}(k) &= \frac{L_f}{R_c T}\left[u_{iqref}(k+1) - u_{iq}(k+1)\right] - \frac{L_f}{R_c}\hat{x}_{2q}(k) \end{aligned} \tag{45}$$

C. Tracking Error of Disturbance Observer

Define the tracking error of the observer as

$$\boldsymbol{e}_{DO} = \boldsymbol{x}_{DO} - \hat{\boldsymbol{x}}_{DO} \tag{46}$$

(41) subtracts (42), we obtain

$$\dot{\boldsymbol{e}}_{DO} = A_e \boldsymbol{e}_{DO} + E\boldsymbol{h} \tag{47}$$

with

$$A_e = A_{DO} - LC_{DO} = \begin{bmatrix} -\beta_{1d} & 0 & 1 & 0 \\ 0 & -\beta_{1q} & 0 & 1 \\ -\beta_{2d} & 0 & 0 & 0 \\ 0 & -\beta_{2q} & 0 & 0 \end{bmatrix}.$$

The characteristic polynomial of A_e is

$$\begin{aligned} f(\lambda) = \lambda^4 + \left(\beta_{1d} + \beta_{1q}\right)\lambda^3 + \left(\beta_{2d} + \beta_{2q} + \beta_{1d}\beta_{1q}\right)\lambda^2 + \\ \left(\beta_{1d}\beta_{2q} + \beta_{1q}\beta_{2d}\right)\lambda + \beta_{2d}\beta_{2q} \end{aligned} \tag{48}$$

To guarantee the convergence of the observer tracking errors, all eigenvalues of A_e should be located in the left half plane. Suppose the ideal characteristic polynomial of A_e is $f^*(\lambda) = (\lambda + \omega_0)^4$. Let $f(\lambda) = f^*(\lambda)$, we have $\beta_{1d} = \beta_{1q} = 2\omega_0$, $\beta_{2d} = \beta_{2q} = \omega_0^2$. In this way, not only the eigenvalues of A_e are all negative, but also the adjustment parameter of observer is only ω_0.

D. Stability Analysis

Make the converter voltage derived from MPC (45) equal to the converter voltage derived from observer (15), we can get

$$\begin{aligned} \frac{u_{id}(z)}{u_{idref}(z)} = & \frac{\left(-R_c^2T^2 + L_f L_{f0}\right)z^3}{\left(-R_c^2T^2 + L_f L_{f0}\right)z^3} \\ & \frac{+\left(-2L_f L_{f0} + b_1 L_f L_{f0} + R_c^2T^2 - b_1 R_c^2 T^2\right)z^2}{+\left(-2L_f L_{f0} + b_1 L_f L_{f0} + R_c^2T^2 - b_1 R_c^2 T^2\right)z^2} \\ & \frac{+\left(L_f L_{f0} - b_1 L_f L_{f0}\right)z}{+\left(L_f L_{f0} - b_1 L_f L_{f0} - Tb_2 L_f L_{f0}\right)z + Tb_2 L_f L_{f0}} \end{aligned} \tag{49}$$

The poles and zeros of (49) are shown in Fig. 4. There is always a zero and pole close to 1, and they do not change with the observer gains. In Fig. 4(a), the other poles shift away from center while $b_1 = 1$ and b_2 changes from 0 to 100. In Fig. 4(b), one pole moves toward center, the other moves toward unit circle while $b_2 = 4000$ and b_1 changes from 0.1 to 2. The system's stability is affected by b_1 and b_2. We chose $b_1 = 1.3$ and $b_2 = 4000$ as a balance between reaction speed and stability.

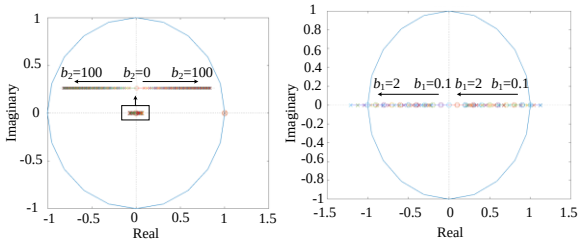

(a) (b)

Fig. 4 The poles and zeros of (49).

The proposed control for *LCL*-filtered grid converter is shown in Fig. 5. The phase locked loop (PLL) is adopted to obtain the grid voltage phase angle. The MPC of the *LC* filter includes two parts. The first one is the predictive model of interconnection voltage $u_{id}(k+1)$ and $u_{iq}(k+1)$. Then the predicted interconnection voltage is delivered to the second part which calculates the converter voltage $u_{fd}(k)$ and $u_{fq}(k)$. For compensating the lump of disturbances, the converter voltage and the interconnection voltage at k^{th} period are delivered to the disturbance observer which estimates the disturbances to calculate the converter voltage.

IV. Proposed PR and MPC of Grid Converters

A. Proportional Resonance Control of the Grid Side Current

PR controls the grid side current with zero steady state error. However, the PR controller only works at a single frequency. Due to the uncertainty of measurement and sampling, quasi proportional resonant (QPR) will be used to replace PR. The transfer function of QPR is

$$G_{QPR}(s) = k_{pr} + \frac{2k_{ir}\omega_c s}{s^2 + 2\omega_c s + \omega_1^2} \tag{50}$$

where k_{pr} and k_{ir} are the proportional and resonance gain, ω_c and ω_1 are the cutoff and fundamental frequency.

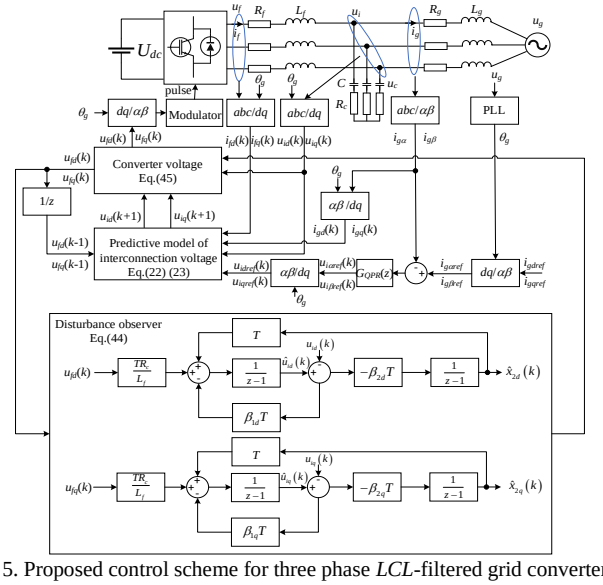

Fig. 5. Proposed control scheme for three phase *LCL*-filtered grid converter.

Substitute $s=\omega_1(z-1)/\left[\tan(\omega_1 T/2)(z+1)\right]$ into (50), the discrete transfer function of QPR is

$$G_{QPR}(z)=k_{pr}+k_{ir}\omega_c\sin(\omega_1 T)\frac{z^2-1}{(\omega_1+\omega_c\sin(\omega_1 T))z^2-2z\omega_1\cos(\omega_1 T)+\omega_1-\omega_c\sin(\omega_1 T)} \quad (51)$$

where T is the sampling time.

B. Frequency Response of the Proposed Control

The block diagram of the proposed control is shown in Fig. 6 (c).

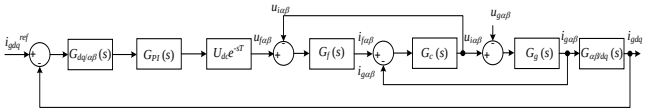

(a) Conventional PI current control without active damping.

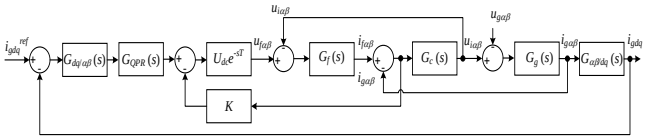

(b) PR current control with active damping.

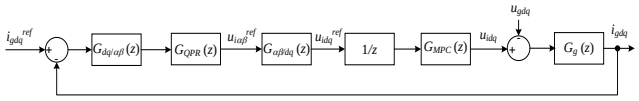

(c) Proposed PR and model predictive control.

Fig. 6. Block diagram of the PI control, PR control and proposed control.

$G_{dq/\alpha\beta}(s)$ is the continuous transfer function matrix from dq components to the $\alpha\beta$ components [23]. $G_{dq/\alpha\beta}(z)$ is the discrete form of $G_{dq/\alpha\beta}(s)$.

$$G_{dq/\alpha\beta}(s)=\begin{bmatrix}1 & 0\\ 0 & 1+u_{gd}T_{PLL}(s)\end{bmatrix} \quad (52)$$
$$T_{PLL}(s)=\frac{G_{PLL}(s)}{s+u_{gd}G_{PLL}(s)}$$

where $G_{PLL}(s)=k_{ppll}+k_{ipll}/s$ is the PLL PI control.

$G_{\alpha\beta/dq}(s)$ is the continuous transfer function matrix from $\alpha\beta$ components to the dq components. $G_{\alpha\beta/dq}(z)$ is the discrete form of $G_{\alpha\beta/dq}(s)$.

$$G_{\alpha\beta/dq}(s)=\begin{bmatrix}1 & 0\\ 0 & 1-u_{gd}T_{PLL}(s)\end{bmatrix} \quad (53)$$

The MPC with disturbance observer is nonlinear and discontinuous, hence it is hard to obtain its frequency response. Harmonic balance method [24] is an approximately equivalent linearization representation in frequency domain.

The system parameters are listed in Table I. The discrete transfer function of MPC is

$$G_{MPC}(z)=\frac{-0.08139z^3-0.7233z^2-0.5432z-0.03706}{z^4-4.459z^3+3.313z^2-1.516z+0.278} \quad (54)$$

The transfer function of the grid side inductor is

$$G_g(s)=\frac{1}{L_g s+R_g} \quad (55)$$

The zero-order hold is used to discretize $G_g(s)$.

$$G_g(z)=(1-z^{-1})Z\left(\frac{G_g(s)}{s}\right)=\frac{1}{R_g}\frac{1-e^{-R_g T/L_g}}{z-e^{-R_g T/L_g}} \quad (56)$$

The open loop transfer function of the grid side current in dq axis is

$$G_{pd}(z)=z^{-1}G_{QPR}(z)G_{MPC}(z)G_g(z) \quad (57)$$
$$G_{pq}(z)=z^{-1}\left(1+u_{gd}T_{PLL}(z)\right)G_{QPR}(z)G_{MPC}(z)G_g(z)\left(1-u_{gd}T_{PLL}(z)\right)$$

The closed-loop output impedance of three phase LCL-filtered converter contains d-axis and q-axis components is

$$Z_{pd}(z)=\frac{u_{gd}}{-i_{gd}}=\frac{1+G_{pd}(z)}{G_g(z)} \quad (58)$$
$$Z_{pq}(z)=\frac{u_{gq}}{-i_{gq}}=\frac{1+G_{pq}(z)}{G_g(z)}$$

TABLE I.
SYSTEM PARAMETERS

Symbol	Variables	Value
U_{dc}	DC side reference voltage	500 V
T	Sampling time	50 μs
L_f	Converter side inductance	1 mH
R_f	Converter side parasitic resistance	0.1 Ω
L_g	Grid side inductance	0.8 mH
R_g	Grid side parasitic resistance	0.1 Ω
C	Filter capacitance	20 μF
R_c	Charging resistance	0.001 Ω
k_{pr}	PR proportional gain	10
k_{ir}	PR resonance gain	1000
k_{ppll}	PLL proportional gain	5
k_{ipll}	PLL integral gain	50
u_q	Rated grid voltage	200 V
ω_1	Fundamental frequency	50 Hz
f_s	Switching frequency	5 kHz

For comparison, the block diagram of PI current control without active damping and PR current control with active damping are shown in Figs. 6 (a) and 6 (b). The Bode diagram of open loop transfer function in (57) is shown in Fig. 7. Since G_{pd} does not involve PLL, the change of PLL gains has no effect on it. When PLL gains become larger, the phase margins of G_{pq} increase. Hence the oscillation induced by PLL can be avoided by selecting appropriate PLL gains.

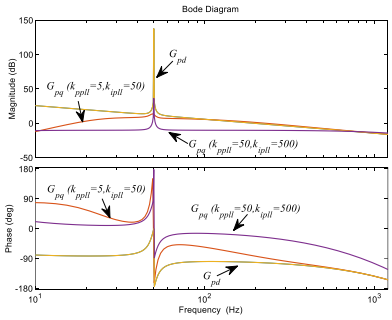

Fig. 7. Bode Diagram of open loop transfer function in (57).

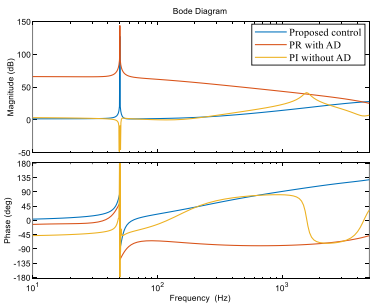

Fig. 8. Bode Diagram of output impedance of three control schemes.

The frequency response of output impedance of three controls are shown in Fig. 8. It can be found that the phase-frequency response of PR and PI control are -90 degrees in the high frequency, which means that output impedance is capacitive and high frequency oscillation may occur when the converter is connected to inductive AC grid. The output impedance of PI control is capacitive in the frequency lower than 50 Hz and may cause subsynchronous oscillation. The phase-frequency response of the proposed control is not in the capacitive region which is from -180° to 0°, hence subsynchronous oscillation and high frequency oscillation will not occur in the proposed control. The Bode diagrams of open loop transfer function of three controls are shown in Fig. 9. It can be seen that the proposed control can inherently restrain the high frequency resonance peak without additional damping. Since active damping based on the feedback of capacitor current is adopted in PR control, there is no high frequency resonance peak in PR control. However, the phase margin of PR control is almost zero, which is easy to cause instability.

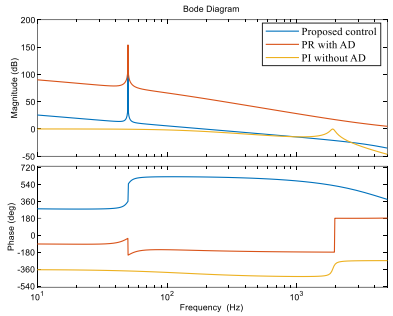

Fig. 9. Bode Diagram of open loop transfer functions of three control schemes.

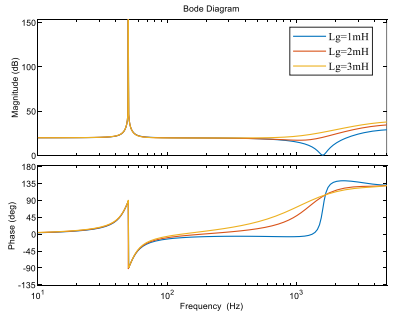

Fig. 10. Impact of grid side inductance on the proposed control.

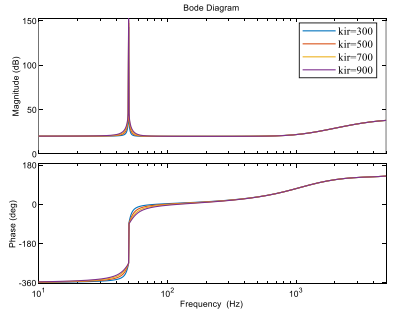

Fig. 11. Impact of PR resonance gain on the proposed control.

The Bode diagram of output impedance of the proposed control under different grid side inductance is shown in Fig. 10. We see that the variation of grid side inductance only affects the frequency response in high frequency range. As the grid side inductance increases, the output impedance of the proposed control changes from resistive to inductive, and high frequency oscillation will not occur.

The Bode diagrams of output impedance of the proposed control under different PR resonance gain are shown in Fig. 11. It can be found that PR resonance gain has little effect on the output impedance. The output impedance is resistive in the subsynchronous frequency domain and inductive in the high-frequency domain, hence subsynchronous oscillation and high frequency oscillation will not occur.

The Bode diagrams of output impedance of the proposed control under different PR proportional gain are shown in Fig. 12. It can be found that PR proportional gain has little impact on the output impedance in low and middle frequency, where the output impedance is resistive and oscillations at these frequencies will not occur. As PR proportional gain increases, the output impedance is always resistive-inductive in high frequency and high frequency oscillation is eliminated.

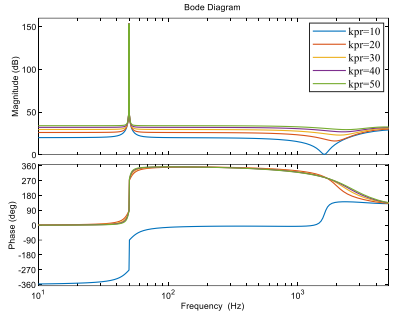

Fig. 12. Impact of PR proportional gain on the proposed control.

From Fig. 10-12, we can conclude that the proposed control has strong robustness to the variations of grid side inductance and PR control gains, and inherently mitigates subsynchronous oscillation and high frequency oscillation.

V. Simulation Results of Proposed Control

A. *Performance Under the Condition of Step Current*

Three phase grid side currents and their total harmonic distortions (THD) using the proposed control and PR control with active damping are shown in Figs. 13 and 14. It can be seen that THD is reduced greatly under the proposed control. This is consistent with the frequency response in Fig. 8 where the phase margin of the proposed control is much more sufficient than PR control with active damping. And the output impedance of the proposed control is resistive or inductive in the full frequency which mitigates the oscillation.

When the *d*-axis grid side current reference steps from 100A to 150A, phase A current of the proposed control and PR control with active damping are shown in Figs. 15 (a) and 15(b). It can be seen that the current tracking effect of the proposed control is better when the current reference is stepped. Compared with PR control with active damping, MPC has better dynamic and static performances.

This article has been accepted for publication in IEEE Transactions on Industry Applications. This is the author's version which has not been fully edited and content may change prior to final publication. Citation information: DOI 10.1109/TIA.2022.3228972

As shown in Figs. 16 and 17, when the grid side inductance varies from 0.1mH to 0.5mH, the grid side current of PR control with active damping is heavily distorted, which impacts the power quality seriously. However, the proposed control can keep the stable operation of the converter when the grid side inductance varies and ensure good power quality of the grid side current. The simulation results are consisted with the frequency response analysis in Fig. 10, which verifies the proposed control has strong robustness to the disturbances.

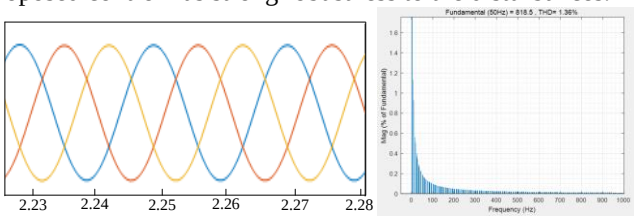

(a) Three phase grid side current. (b) THD=1.36%.

Fig. 13. Grid side currents and FFT analysis of the proposed control.

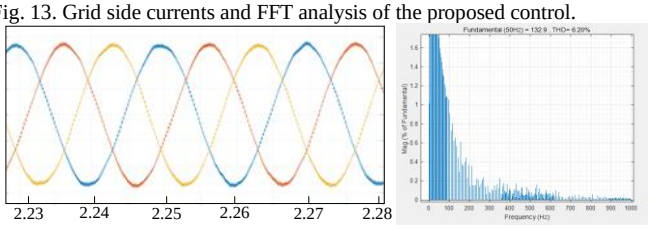

(a) Three phase grid side current. (b) THD=6.20%

Fig. 14. Grid side currents and FFT analysis of the PR control with active damping.

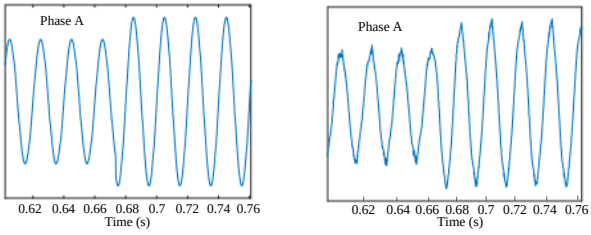

(a) Proposed control. (b) PR control with active damping.

Fig. 15. Phase A grid side current for grid side current reference step changes.

B. Control Parameters and Steady-state Analysis of The Improved Model Predictive Control

In order to assess the on-off frequency of the improved model predictive control, we define the average frequency of switching as:

$$f_{asw} = \left(t_{swa} + t_{swb} + t_{swc}\right)/3T \tag{59}$$

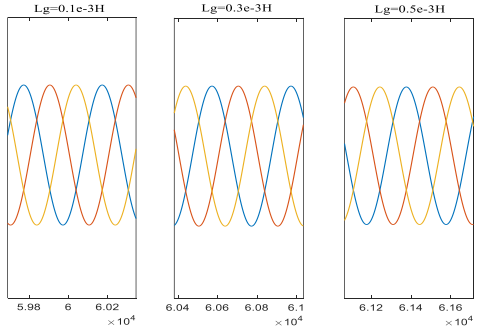

Fig. 16. Impact of grid side inductance on gird side current of the proposed control.

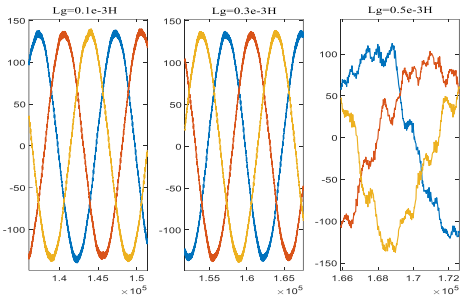

Fig. 17. Impact of grid side inductance on gird side current of PR control with active damping.

where $T = 0.2$s is the computing cycle of the average frequency of switching, t_{swa}, t_{swb}, t_{swc} are the switching times of phase a, b, and c in T.

For the purpose of finding out the optimal configuration of control parameters, the effect of the weighted factors λ_{dif}, λ_{sw}, and the feedback compensation factor λ_c on the capacitor voltage THD and the average frequency of switching are investigated. λ_{dif} is varied from 0 to 1, and λ_{sw} is varied from 0 to 5, when λ_c is 0.5 and 1.

As shown in Fig. 17, the capacitor voltage THD alleviates as λ_{dif} increases, and aggravates as λ_{sw} increases. When the feedback compensation factor λ_c increases, the capacitor voltage THD reduces and the control effect is enhanced under different configuration of λ_{dif} and λ_{sw}.

Moreover, it can be observed from Fig. 18 that the average frequency of switching raises as λ_{dif} increases, and reduces as λ_{sw} increases. Combined with the simulation analysis shown in Figs. 18 and 19, we can determine the optimal configuration of control parameters.

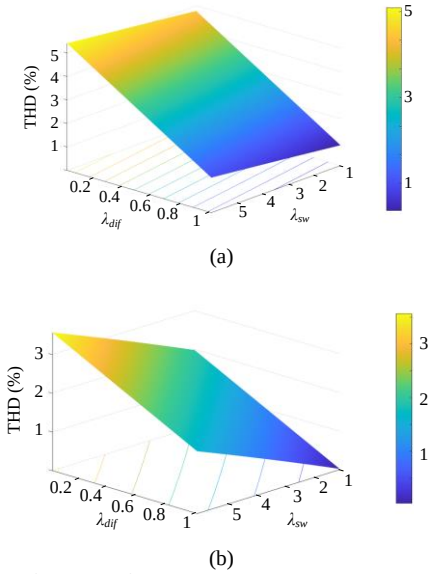

(a)

(b)

Fig. 18. Impact of weighted factors λ_{dif} and λ_{sw} on the capacitor voltage THD. (a) $\lambda_c = 0.5$. (b) $\lambda_c = 1$.

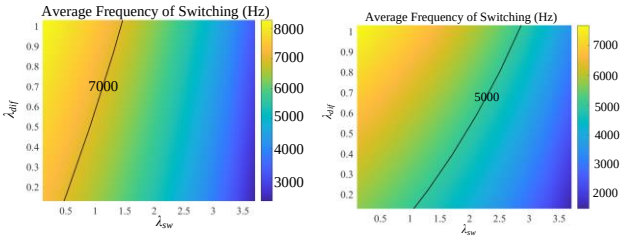

(a) (b)

Fig. 19. Impact of weighted factors λ_{dif} and λ_{sw} on the averaging frequency of switching. (a) $\lambda_c = 0.5$. (b) $\lambda_c = 1$.

VI. Comparison of Real-Time Control Performance

In this section, we use a fully digital real time simulator ADPSS developed by China Electric Power Research Institute to produce a valid real-time simulation to represent the real system correctly. The results of the conventional PI control, overall MPC in [18], and the proposed MPC+PR control are compared.

As shown in Fig. 20, when $i_{gdref} = 150\text{A}$, the grid side current at *d*-axis i_{gd} arrives at the reference value most fast under the proposed control. The overshoot under the proposed control is much less than that under PI and overall MPC. The steady state current vibration under the proposed control is the smallest of the three controls. When compared to PI control and overall MPC, the proposed control exhibits quicker response and superior dynamic performance.

In Fig. 21, the proposed control produces less high-order harmonics than PI control and overall MPC, which significantly reduces the capacitor current distortion.

To further verify the control performance, simulations under step change of *d*-axis grid side current reference are performed. Fig. 22 displays i_{gd} when i_{gdref} steps from 100A to 150A. At 0.3 s, when i_{gdref} changes, the proposed control outperforms the overall MPC in terms of decoupling of *d*-axis and *q*-axis currents as well as response speed.

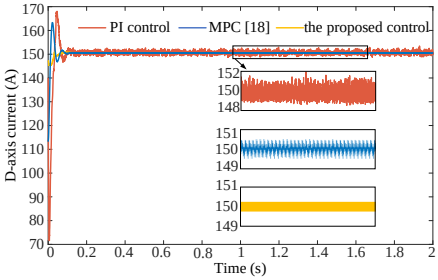

Fig. 20 Grid side current at *d*-axis under three control methods.

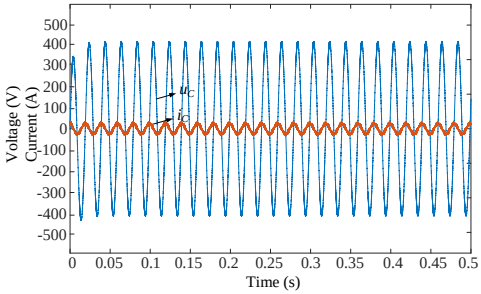

(a) Under the proposed control.

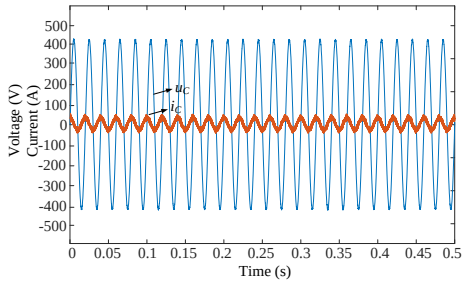

(b) Under MPC in [18].

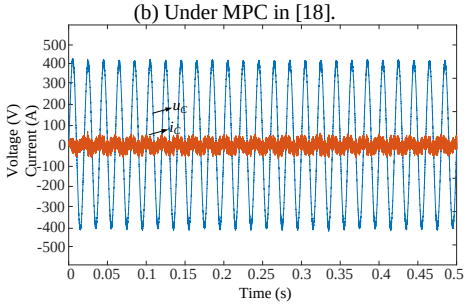

(c) Under conventional PI control.

Fig. 21 Capacitor voltage and current under three control methods.

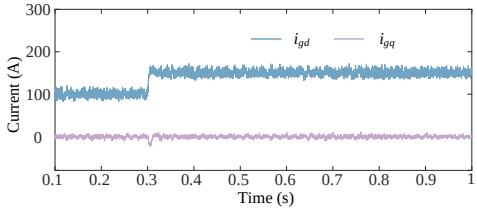

(a) Under MPC in [18].

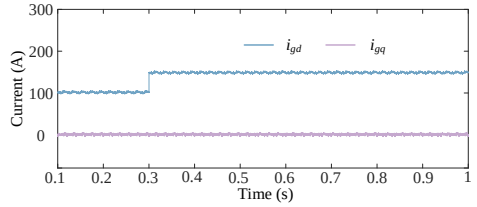

(b) Under the proposed control.

Fig. 22 The response under step change of grid side current reference.

VII. Conclusion

We propose a robust control scheme for three phase *LCL*-filtered gird converters to reduce high frequency and subsynchronous or supersynchronous oscillations in this paper. The interconnection voltage of *LC* filter is regulated by MPC with disturbance observer. The grid side current is regulated by PR control. MPC can inherently realize active damping without additional control and reduce modulation delay, which improves the dynamic performance. PR control not only makes the steady state error zero, but also reduces the complexity of control compared with the overall grid converter is controlled by MPC. Simulation results show that THD of the grid side current is reduced greatly under the proposed control. The current tracking of the proposed control is better when the current reference is stepped. The proposed control also can keep the stable operation of the converter when the grid side inductance varies and ensure good power quality of the grid side current. Moreover, we proposed an improved MPC control framework and a feedback compensation method for MPC to

enhance delay synchronization and output prediction, therefore reducing the tracking error and the resulting oscillations and harmonics. Compared with PI control, PR control, and overall MPC, the proposed control has better dynamic and static performances.

APPENDIX A

The state-space model of *LC* filter is

$$L_f \frac{di_{fd}}{dt} = u_{fd} - u_{id} - R_f i_{fd} + \omega_s L_f i_{fq} \tag{A1}$$
$$= u_{fd} - u_{cd} - \left(R_f + R_c\right) i_{fd} + R_c i_{gd} + \omega_s L_f i_{fq}$$

$$L_f \frac{di_{fq}}{dt} = u_{fq} - u_{iq} - R_f i_{fq} - \omega_s L_f i_{fd} \tag{A2}$$
$$= u_{fq} - u_{iq} - \left(R_f + R_c\right) i_{fq} + R_c i_{gq} - \omega_s L_f i_{fd}$$

$$C \frac{du_{cd}}{dt} = i_{fd} - i_{gd} + \omega_s C u_{cq} \tag{A3}$$

$$C \frac{du_{cq}}{dt} = i_{fq} - i_{gq} - \omega_s C u_{cd} \tag{A4}$$

$$\frac{di_{gd}}{dt} = d_{gd} \tag{A5}$$

$$\frac{di_{gq}}{dt} = d_{gq} \tag{A6}$$

The output variable is the interconnection voltage:

$$u_{id} = R_c i_{fd} - R_c i_{gd} + u_{cd} \tag{A7}$$

$$u_{iq} = R_c i_{fq} - R_c i_{gq} + u_{cq} \tag{A8}$$

The dynamics of the grid side current is

$$L_g \frac{di_{gd}}{dt} = u_{id} - u_{gd} - R_g i_{gd} + \omega_s L_g i_{gq} \tag{A9}$$

$$L_g \frac{di_{gq}}{dt} = u_{iq} - u_{gq} - R_g i_{gq} + \omega_s L_g i_{gd} \tag{A10}$$

REFERENCES

[1] Q. Geng, X. Zhou, H. Sun and X. Zhang, "Mitigation of Oscillations in Grid Converters Enabled Microgrids Based on Proportional Resonance and Model Predictive Control," 2021 IEEE/IAS Industrial and Commercial Power System Asia (I&CPS Asia), 2021, pp. 665-673.

[2] N. Pogaku, M. Prodanovic, and T. C. Green, "Modeling, analysis and testing of autonomous operation of an inverter-based microgrid," *IEEE Trans. Power Electron.*, vol. 23, no. 6, pp. 2806-2816, Nov. 2008.

[3] Y. W. Li, "Control and resonance damping of voltage source and current source converters with LC filters," *IEEE Trans. Ind. Electron.*, vol. 56, pp. 1511-1521, May 2009.

[4] J. M. Carrasco, L. G. Franquelo, J. T. Bialasiewicz *et al*, "Power electronic systems for the grid integration of renewable energy sources: A survey," *IEEE Trans. Power Electron.*, vol. 53, no. 4, pp. 1002-1016, Aug. 2006.

[5] J. Enslin and P. Heskes, "Harmonic interaction between a large number of distributed power inverters and the distribution network," *IEEE Trans. on Power Electron.*, vol. 19, pp. 1586-1593, Nov. 2004.

[6] J. Dannehl, C. Wessels, and F. W. Fuchs, "Limitations of voltage-oriented PI current control of grid-connected PWM rectifiers with LCL filters," *IEEE Trans. Ind. Electron.*, vol. 56, no. 2, pp. 380-388, Feb. 2009.

[7] M. Liserre, F. Blaabjerg, and S. Hansen, "Design and control of an lcl-filter-based three-phase active rectifier," *IEEE Trans. on Ind. Appl.*, vol. 41, no. 5, pp. 1281-1291, 2005.

[8] R. B. Gonzatti, S. C. Ferreira, C. H. da Silva *et al*, "Using Smart Impedance to Transform High Impedance Microgrid in a Quasi-Infinite Busbar," *IEEE Trans. on Smart Grid*, vol. 8, no. 1, pp. 428-436, Jan. 2017.

[9] M. Liserre, R. Teodorescu, and F. Blaabjerg, "Stability of photovoltaic and wind turbine grid-connected inverters for a large set of grid impedance values," *IEEE Trans. Ind. Appl.*, vol. 42, no. 5, pp. 1146-1154, Sep. 2006.

[10] S. Munir and Y. W. Li, "Residential Distribution System Harmonic Compensation Using PV Interfacing Inverter," *IEEE Trans. on Smart Grid*, vol. 4, no. 2, pp. 816-827, June 2013.

[11] R. Pena-Alzola, M. Liserre, F. Blaabjerg *et al*, "A self-commissioning notch filter for active damping in a three-phase lcl-filter-based grid-tie converter," *IEEE Trans. on Power Electron.*, vol. 29, pp. 6754-6761, Dec. 2014.

[12] M. Liserre, R. Teodorescu, and F. Blaabjerg, "Multiple harmonics control for three-phase grid converter systems with the use of PI-RES current controller in a rotating frame," *IEEE Trans. Power Electron.*, vol. 21, no. 3, pp. 836-841, May 2006.

[13] J. Dannehl, M. Liserre, and F. W. Fuchs, "Filter-based active damping of voltage source converters with lcl filter," *IEEE Trans. on Ind. Electron.*, vol. 58, pp. 3623-3633, Aug. 2011.

[14] J. Dannehl, F. W. Fuchs, S. Hansen, and P. B. Thogersen, "Investigation of active damping approaches for pi-based current control of grid connected pulse width modulation converters with lcl filters," *IEEE Trans. on Ind. Appl.*, vol. 46, pp. 1509-1517, Jul. 2010.

[15] Y. Tang, P. C. Loh, P. Wang *et al*, "Exploring inherent damping characteristics of LCL-filters for three-phase grid-connected voltage source inverters," *IEEE Trans. Power Electron.*, vol. 27, no. 3, pp. 1433-1443, Mar. 2012.

[16] F. Liu, S. Duan, J. Yin, B. Liu, and F. Liu, "Parameter design of a two current-loop controller used in a grid-connected inverter system with LCL filter," *IEEE Trans. Ind. Electron.*, vol. 56, no. 11, pp. 4483-4491, Nov. 2009.

[17] S. Mariethoz, M. Morari, "Explicit model-predictive control of a PWM inverter with an LCL filter," *IEEE Trans. Ind. Electron.*, vol. 56, no. 2, pp. 389-399, Feb. 2009.

[18] S. C. Ferreira, R. B. Gonzatti, R. R. Pereira *et al*, "Finite control set model predictive control for dynamic reactive power compensation with hybrid active power filters," *IEEE Trans. Ind. Electron.*, vol. 65, no. 3, pp. 2608-2617, Mar. 2018.

[19] N. Panten, N. Hoffmann, and F. W. Fuchs, "Finite control set model predictive current control for grid-connected voltage-source converters with lcl filters: A study based on different state feedbacks," *IEEE Trans. on Power Electron.*, vol. 31, pp. 5189-5200, Jul. 2016.

[20] J. Scoltock, T. Geyer, and U. K. Madawala, "A model predictive direct current control strategy with predictive references for mv grid-connected converters with lcl-filters," *IEEE Trans. on Power Electron.*, vol. 30, pp. 5926-5937, Oct. 2015.

[21] C. S. Lim, S. S. Lee, I. U. Nutkani *et al*, "Near-optimal MPC algorithm for actively damped grid-connected PWM-VSCs With LCL filters," *IEEE Trans. Ind. Electron.*, vol. 67, no. 6, pp. 4578-4589, Jun. 2020.

[22] M. Tomlinson, H. D. T. Mouton, R. Kennel, and P. Stolze, "A fixed switching frequency scheme for Finite-Control-Set model predictive control-Concept and algorithm," IEEE Trans. Ind. Electron., vol. 63, no. 12, pp. 7662-7670, Dec. 2016.

[23] J. Dannehl, C. Wessels, and F. W. Fuchs, "Limitations of voltage-oriented PI current control of grid-connected PWM rectifiers with LCL filters," *IEEE Trans. Ind. Electron.*, vol. 56, no. 2, pp. 380–388, Feb. 2009.

[24] Y. Song, F. Blaabjerg, "Analysis of middle frequency resonance in DFIG system considering phase-locked loop," *IEEE Trans. on Power Electron.*, vol. 33, no. 1, pp. 343-356, Jan. 2018.

[25] A. Gelb and W. Velde, Multiple-Input Describing Functions and Nonlinear System Design. McGraw-Hill, 1968.